Advances in Military Technology
Vol. 17, No. 1, 2022, pp. 17-32
ISSN 1802-2308, eISSN 2533-4123
DOI 10.3849/aimt.01523

Design and Numerical Analysis of a Plug Nozzle

S. Haif,* H. Kbab and A. Benkhedda

Université de Blida 1, Aeronautics and Space Studies Institute, Aeronautical Sciences Laboratory, Blida, Algeria

The manuscript was received on 10 August 2021 and was accepted after revision for publication as research paper on 13 March 2022.

Abstract:

The purpose of this study is to simulate the flow in the plug nozzle. Further, the evolution of the parameters of this flow was studied. The mass of the nozzle and of the exhaust gases was calculated by the simulation. In addition, all these results are then compared with those obtained by the numerical calculations. In the second part of the study, the method of an approximate method was used to generate the profile of the plug nozzle for different values of heat capacity ratio γ and the number of exit Mach. Finally, our results are compared with those obtained numerically and experimentally (available in open literature).

Keywords:

approximate method, aerospike, fluent ANSYS, function of Prandtl Meyer, plug nozzle

1 Introduction

Most liquid propellant engines used on launchers are equipped with fixed geometry nozzles. These types of nozzles limit engine performance as they operate at optimum efficiency at a single point along the flight path. Conversely, a nozzle with a variable cross-section ratio optimizes the pulse delivered throughout the flight path: Several advanced nozzle concepts have been studied for this purpose [1]. Among these nozzles, (Aerospike) is a self-adaptive nozzle with altitudes for one-stage in orbit (SSTO) applications [2].

The full-length two-dimensional plug nozzle has a continuously expanding flow, while in off-design conditions, it has wave interactions in the central jet flow. On the contrary, the truncated plug nozzles present complexities of the base flow and its transition in addition to wave interactions in the flow of the central jet. Therefore, the design of plug nozzles with such complex flow physics continues to pose a challenge to the aerospace community [3]. It is in this context that the role of predictive tools such as empirical models and computational fluid dynamics (CFD) becomes important.

* *Corresponding author: Aeronautics and Space Studies Institute, Aeronautical Sciences Laboratory, BP270 Route De Soumàa, Blida, Algeria. Phone: +213 6 72 03 86 71, E-mail: haifsidali06@gmail.com*

To fully understand the aerospike nozzle, we compared two methods of designs of these nozzles for different M_E and γ, and attempted to validate the CFD for complete length and truncated Aerospike nozzle flows with custom experiments for a range of P_R (Chamber Pressure P_0 / Ambient Pressure P_a).

2 The Literature Review

The plug nozzle concept was first developed by the Germans prior to World War II for aeronautical applications. Plug nozzles have a central body in the vicinity of the neck and the process of gas expansion is directly or indirectly regulated by ambient pressure, the gas flow is regulated by detent waves from the flow deviation due to the plug surface [1]. Based on weight/thrust ratio considerations, the cap is generally truncated, resulting in a very complex base flow. The use of these nozzles in the past was very rare, for example the Second World War fighter aircraft named Messerschmitt Me 262 was equipped with annular plug nozzle.

For the first time in 1950, Griffith of Rolls-Royce, Ltd., proposed the concept of plug nozzle for rocket propulsion in an American patent [4]. In 1959, Krase was the first to propose methods to designate ideal plug nozzle contours by simple approximate calculations [5]. In 1961, Berman and Cromp made studies on the modification of the end of plug and they found out that if half-cone angles at the end of the plug are used, a decrease in performance is of only 1 % [6]. In the same year, Rao discussed the use of plug contour optimization as the case in the conventional nozzle and obtained optimal contours [7]. In 1964, Angelino described an approximate method for axisymmetrical and two-dimensional plug nozzle design based on a simple technique [8]. Balasaygun studied the difference in performance between the plug nozzles and the conventional nozzles, and he found out that the nature of the flow in the plug nozzles is auto-adjustable, resulting in better performance when the nozzle is operated at a lower pressure ratio than the design [9]. In 1974, Johnson et al presented an optimization analysis for axial plug nozzles with variable input geometry [10].

The improvement in the efficiency of numerical simulation has led to the extensive study of this type of nozzle. The first numerical simulation was in 1997, Rommel et al. studied the development of the flow field as a function of ambient pressure variations using a computer study of a plug nozzle [11]. To minimize weight, McConnaughey conducted a numerical study of a three-dimensional aerospike and concluded that a 50 % truncation of the plug nozzle resulted in a 0.5 % reduction in performance only [12]. In 1998, Hagemann et al. carried out a numerical study based on the method of characteristics for the flow field simulations of plug nozzles, and they discussed the flow phenomena observed in experiments and numerical simulations of different adaptive plug nozzles in altitude [13]. In 2002, Ito et al. studied flow structures and thrust performance of axisymmetric truncated plug nozzles using a numerical simulation. They obtained a high gain from the plane plug nozzle (aerospike) of about 5 % to 6 % compared to the axisymmetric plug nozzle and for pressure ratios greater than the design ratio, the pressure distribution on the nozzle wall was not affected by the external flow [14]. Besnard et al. presented the manufacture, design and testing of a thrust engine equal to 1 000 lbf (4 448 N) of plug nozzle type. Their results showed that variations in heat capacity ratio led to a difference in thrust characteristics [15]. In 2006, using the Prandtl Meyer function for different specific heat ratios, Zebbiche plotted the profiles of the plug nozzle. Comparing the obtained performance with an MNL (Minimum Length Nozzle), he concluded that plug nozzles perform better [16]. In 2010, Shahrokhi

and Noori used CFD to study the different flow properties of Aerospike nozzle [17]. In 2012, Karthikeyan et al. studied the effect of plug truncation of an aerospike nozzle on acoustic behavior [18]. In 2014, Chutkey et al. conducted a numerical and experimental study on the behavior of flow fields at truncated annular plug nozzle of different lengths [19].

In recent years, starting in the year 2015, Shanmuganathan et al. conducted a numerical comparative study on linear and annular plug nozzles and concluded that the annular nozzle was better than the linear nozzle [20]. In 2017, Kumar et al. compared the full length to the optimized plug nozzle models and discussed the aerospike nozzle design procedure and the parameters governing its design [21]. In 2019, Suryan et al. did a two-dimensional axisymmetric numerical analysis on flow through truncated conical plug nozzles with the introduction of a base bleed. They found that the introduction of the base bleed compensates for the loss of thrust due to the truncation of the conical supersonic plug nozzle [22]. In 2020, numerical simulations on an annular nozzle fed by a toroidal combustion chamber were carried out by Ferlauto et al. [23], in order to understand what are the main phenomena that affect the interaction between the primary flow and the injection of secondary flow on the truncated plug. In particular, the location of the injection orifice was studied. In 2021, Alshiya et al. did an experimental study on a plug aerospike nozzle in terms of pressure through an experimental setup of a jet flow apparatus with the assistance of CFD results in order to the reduction of potential core length. They also demonstrated that the spike configuration results in improvement of efficiency compared to C-D nozzle. The study was carried out on an aerospike nozzle with a 15° half-angle conical plug [24].

3 Methodology

In this section, we will discuss the design process of two-dimensional plug nozzles discussed in reference [16]. The design method is based on the function of Prandtl Meyer.

$$v(M) = \sqrt{\frac{\gamma+1}{\gamma-1}} \arctan \sqrt{\frac{\gamma-1}{\gamma+1}\left(M^2-1\right)} - \arctan\sqrt{M^2-1} \tag{1}$$

The number of Mach $M = 1.00$ at the throat and it accelerates to the Mach number M_E at the exit section. v is the angle between the velocity vector of the throat and the x-axis.

The lines shown in Fig. 1 represent the Mach waves, they are inclined with angle μ (Angle of Mach), and the flow properties are constant along each line of Mach exits from point A.

Between the line AB and AE, there is an infinity of Mach waves, exit of point A, centered. Each line gives a Mach number; from these lines we can easily deduct a point on the wall (the flow properties are constant along each line of Mach). As the gas is perfect, the velocity vector is tangent with a stream line, which will be regarded as the contour of Plug wall to require (the main idea of this method).

To have a Mach number required at the exit, the flow to the throat must be tilted at an angle θ_B (Flow deviation compared to the horizontal).

DOI 10.3849/aimt.01523

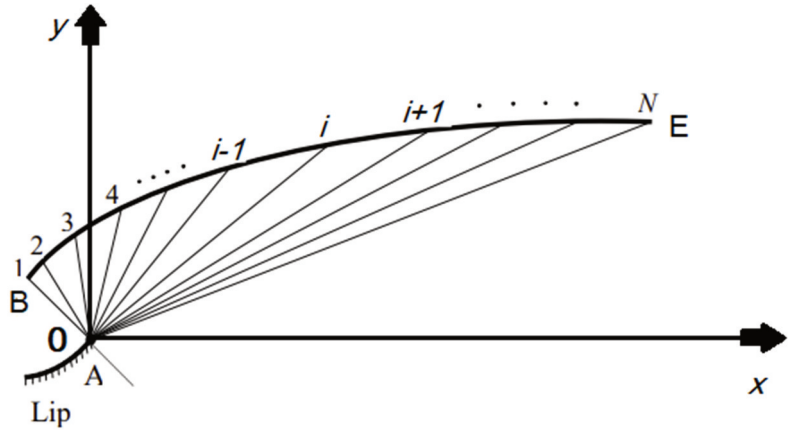

Fig. 1 Discretization of the expansion zone

$$\theta_{\mathrm{B}} = v\left(M_{\mathrm{E}}\right) \tag{2}$$

The Fig. 2 resents the parameters of an intermediate Mach line connecting the point A and point *i*. The determination of wall points is made explicitly.

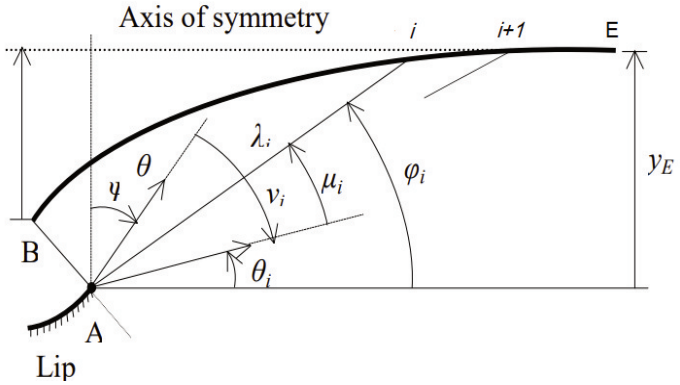

Fig. 2 Parameters of an intermediate Mach

The lines are iso-Mach curves, so the number of Mach in the center of expansion A equals also the number of Mach on the wall. The number of Mach in point *i* is given by:

$$M_i = 1 + (i-1)\left[\left(M_E - 1\right)/\left(N-1\right)\right] \quad \left(i = 1,2,3,\ldots,N\right) \tag{3}$$

where *N* is the selected point number.

Once the number of Mach M_i in point *i* is known. In this case we can write:

$$u_i = \arcsin\frac{1}{M_i} \tag{4}$$

$$v_i = v\left(M_i\right) \tag{5}$$

$$\theta_i = \varphi_i - u_i \tag{6}$$

And for the point $i + 1$ we have:

$$\frac{x_{i+1}}{\lambda_B} = \frac{\lambda_{i+1}}{\lambda_B}\cos\varphi_{i+1} \tag{7}$$

$$\frac{y_{i+1}}{\lambda_B} = \frac{\lambda_{i+1}}{\lambda_B}\sin\varphi_{i+1} \tag{8}$$

λ is the polar ray of a Mach wave with:

$$\frac{\lambda_{i+1}}{\lambda_B} = \frac{\lambda_i}{\lambda_B}\frac{\sin\alpha}{\sin\beta} \tag{9}$$

$$\alpha = \pi - \varphi_i + \nu_E - \nu_i \tag{10}$$

$$\beta = \varphi_{i+1} - \nu_E + \nu_i \tag{11}$$

α and β (angles respectively at tops A and i of the triangle connecting the points A, i and i + 1 of the Fig. 2). φ is the polar angle of Mach.

3.1 The Pressure

The pressure ratio is given by:

$$\left(\frac{P}{P_0}\right)_i = \left(\frac{\rho}{\rho_0}\right)_i \left(\frac{T}{T_0}\right)_i \tag{12}$$

P, ρ and T represent static pressure, density and temperature, respectively, with 0 index for chamber condition.

3.2 The temperature

For the temperature ratio we have:

$$\left(\frac{T}{T_0}\right)_i = \left(1 + \frac{\gamma - 1}{2M_i^2}\right)^{-1} \tag{13}$$

3.3 The Mass of a Plug

Let us suppose that the shape of the wall between two successive points is a straight line, if the number of points N (number of the discretization points of the nozzle wall) is very high. The sum of these lines gives the mass of a plug by:

$$\frac{\text{Mass}}{\rho_M t_M \lambda_B l} = 2\sum_{i=1}^{N-1}\sqrt{\left(\frac{x_{i+1}}{\lambda_B} - \frac{x_i}{\lambda_B}\right)^2 + \left(\frac{y_{i+1}}{\lambda_B} - \frac{y_i}{\lambda_B}\right)^2} \tag{14}$$

ρ_M – the density of a structural material of a plug nozzle,
t_M – the thickness of structural material of a plug nozzle,
l – the unit of nozzle depth,
x, y – Cartesian co-ordinates of a point.

3.4 Pressure Force on the Plug

The axial pressure force exerted on the plug is the sum of all axial pressure forces exerted on all panels.

$$\frac{F_x}{P_0 \lambda_B l} = 2 \sum_{i=1}^{N-1} \left(\frac{P}{P_0} \right)_i \left(\frac{y_{i+1}}{\lambda_B} - \frac{y_i}{\lambda_B} \right) \tag{15}$$

F_x – axial pressure force exerted on the wall of the central body.

3.5 Gas Mass in the Divergent

The mass of gas in the divergent can be considered as the sum of the triangles placed adjacent to each other as shown in Fig. 1, and the uniform area between the Mach AE line and the horizontal.

$$\frac{\text{Mass}_{\text{Gas}}}{\rho_0 \lambda_B{}^2 l} = \left(\frac{\rho}{\rho_0} \right)_E \left[\frac{x_E}{\lambda_B} \frac{y_E}{\lambda_B} \right] + 0.5 \sum_{i=1}^{N-1} \left[\left(\frac{\rho}{\rho_0} \right)_i + \left(\frac{\rho}{\rho_0} \right)_{i+1} \right] \left[\frac{x_{i+1}}{\lambda_B} \frac{y_i}{\lambda_B} - \frac{x_i}{\lambda_B} \frac{y_i}{\lambda_B} \right] \tag{16}$$

4 Results

4.1 Validations of Results with Simulation

In order to validate the calculation method for the plug nozzles [16], we performed a simulation of the flow around the profile of a plug nozzle generated by the reference method [16]. We compared several variables (mass, axial pressure force and gas mass) for M_E = 1.5, 2.0 and 3.0. The results are presented in tabular form. Tabs 1-3 show the comparison between the simulation results and those presented in the reference [16]. The error in the last column of Tabs 1-3 is a relative error calculated using the following formula:

$$\text{Error} = \frac{\text{Numerical results}[1] - \text{Our simulation results}}{\text{Numerical results}[1]} \cdot 100 \tag{17}$$

Tab. 1 Comparison of simulation results with numerical results for M_E = 1.5

	Our simulation	**Numerical results [16]**	**Error [%]**
$\frac{\text{Mass}}{\rho_M t_M \lambda_B l}$	3.07241	3.07504	0.09
$\frac{F_x}{P_0 \lambda_B l}$	0.17781	0.17804	0.13
$\frac{\text{Mass}_{\text{Gas}}}{\rho_0 \lambda_B{}^2 l}$	1.45291	1.45453	0.11

Tab. 2 Comparison of simulation results with numerical results for M_E = 2.0

	Our simulation	**Numerical results [16]**	**Error [%]**
$\frac{\text{Mass}}{\rho_M t_M \lambda_B l}$	6.98860	6.99731	0.12
$\frac{F_x}{P_0 \lambda_B l}$	0.57416	0.57514	0.17
$\frac{\text{Mass}_{Gas}}{\rho_0 \lambda_B{}^2 l}$	2.7963	2.79898	0.10

Tab. 3 Comparison of simulation results with numerical results for M_E = 3.0

	Our simulation	**Numerical results [16]**	**Error [%]**
$\frac{\text{Mass}}{\rho_M t_M \lambda_B l}$	27.2324	27.28409	0.19
$\frac{F_x}{P_0 \lambda_B l}$	1.49447	1.49746	0.20
$\frac{\text{Mass}_{Gas}}{\rho_0 \lambda_B{}^2 l}$	9.03104	9.01751	0.15

By analyzing the values in Tabs 1-3, we can see that our simulation results are in good agreement with the numerical results of the reference [16]. The error rate does not exceed 0.19 % for the mass value, 0.2 % for the value of the axial pressure force, and 0.15 % for the value of the gas mass. This also confirms and demonstrates the ability of CFD (Simulation) solvers to accurately predict flows in the plug nozzle. We also note that the more it increases the number of design Mach M_E, the higher the relative error is.

Figs 3a, 3b and 3c show the wall pressure ratio comparison between the numerical method and the simulation for M_E = 1.5, 2.0 and 3.0 in this order. The results show a good similarity.

Fig. 3d shows the Iso-Pressure contours for a plug nozzle that works in the design Mach number obtained by our simulation. The figure shows the Prandtl–Meyer expansion fan around the lip. In addition, there are no pressure fluctuations or turbulence corresponding to a typical flow along the nozzle of a plug.

Fig. 4 illustrates the mathematical-physical model, the boundary conditions and the mesh adopted for Plug nozzle.

For both M_E = 1.5 and 2.0, the pressure ratio decreases continuously in the divergent before stabilizing at the end of the nozzle, approaching the value of the atmospheric pressure at the tip of the nozzle at a value of 2.5 and 1.25, respectively. On the other hand, for M_E = 3.0, the pressure ratio first falls rapidly at the nozzle

DOI 10.3849/aimt.01523

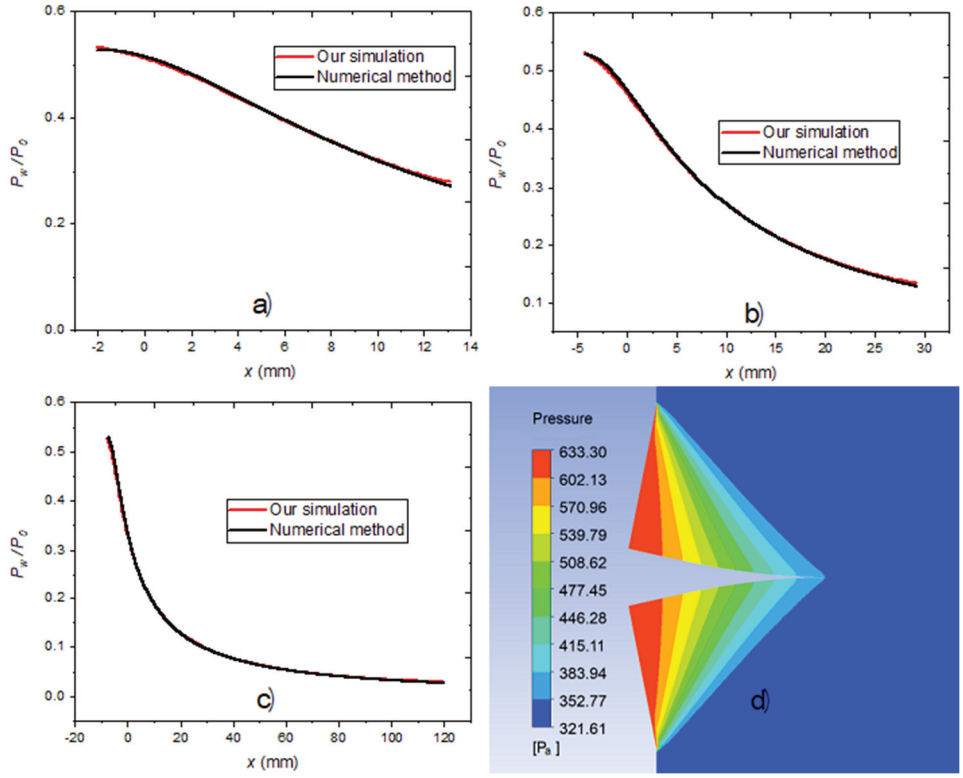

Fig. 3 a) Iso-pressure contours for M_E = 1.5, b) Iso-pressure contours for M_E = 2.0, c) Iso-pressure contours for M_E = 3.0, d) iso-Pressure contours

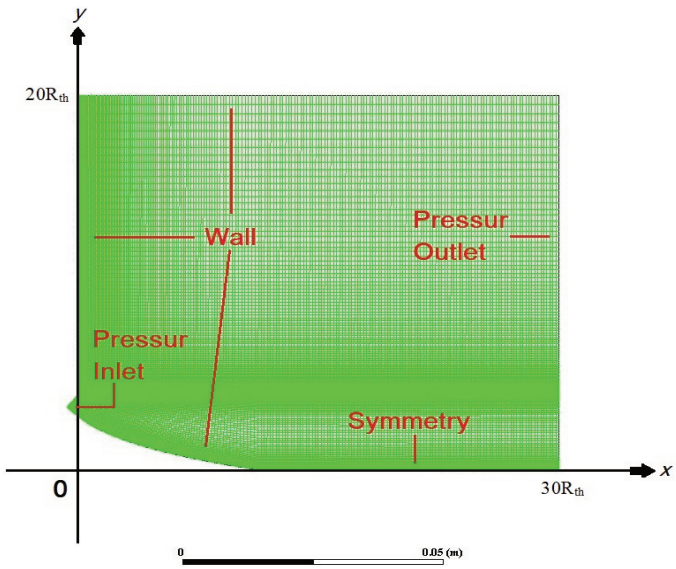

Fig. 4 The mathematical-physics model and the boundary conditions

throat expansion region until it reaches a value of 0.8, then it continues to fall in the expansion part, and then it finally stabilizes at the tip of the nozzle. Regarding this slight drop in pressure at the expansion part, Kbab et al. [25] use a method to reduce the weight of the nozzle without significant impact on the thrust, This is done by truncating the nozzle in the expansion part at a point where the best compromise (weight/performance) is respected. They concluded that if an axisymmetric nozzle is truncated to 79 % of its ideal length, we get a nozzle with a weight gain of 20.85 % and a loss of thrust equal to only 0.987 %.

During the non-viscous calculations, the ambient conditions around the nozzle were modeled by applying a computational domain of $30R_{th}$ in the x-direction by $20R_{th}$ in the y-direction. R_{th} represents the distance between point A and point B (see Fig. 1).

Figs 5a, 5b, and 5c represent the evolution of the Mach number along the wall of the plug nozzle.

Fig. 5d shows the Iso-Mach contours for a plug nozzle that works in the design Mach number obtained by our simulation. It is noted that the flow increases from $M = 1$ in the col until M = design Mach.

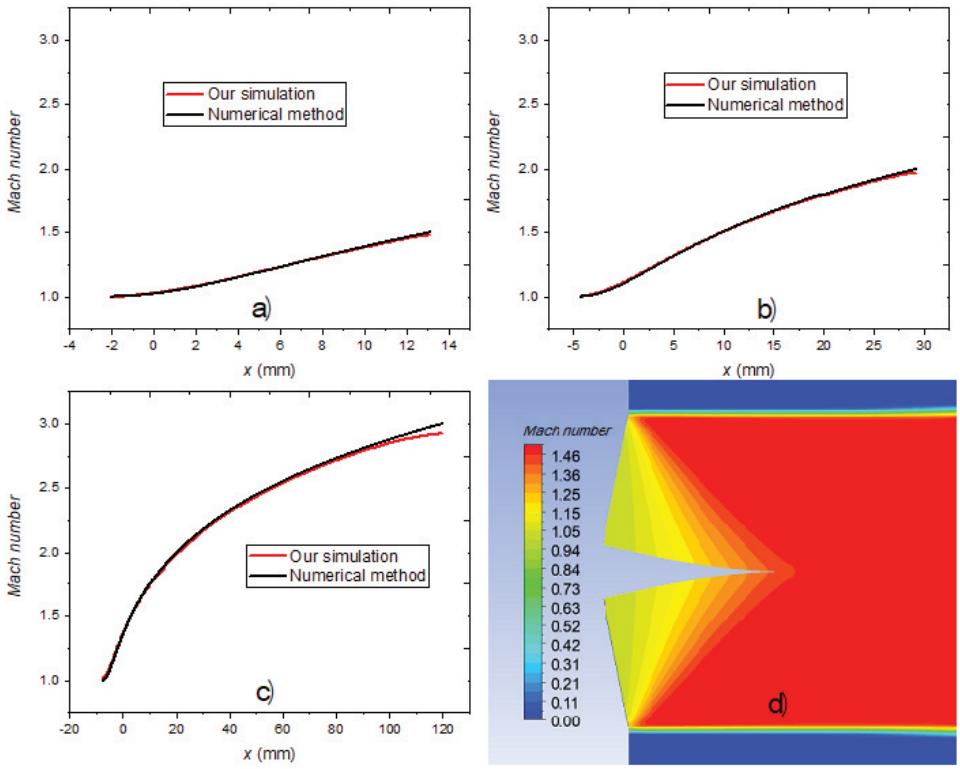

Fig. 5 a) Wall Mach number evolution for M_E = 1.5 b) Wall Mach number evolution for M_E = 2 c) Wall Mach number evolution for M_E = 3.0 d) iso-Mach contours

We note that in the divergent part, the number of Mach increases until reaching the value of the nozzle designing Mach number at the outlet. We notice that the number of Mach at the outlet of the plug nozzle is $M = 1.4$ for nozzle of $M_E = 1.5$ with a length of 11.35 mm. If we truncate the nozzle of $M_E = 3.0$ to a length equal to 11.35 mm, we

obtain a truncated nozzle with the number of Mach at the outlet equal to 1.78. Finally, we have two nozzles of the same length, but different Mach number (weight gain).

4.2 Design Method Validation

In this part the design method is validated by comparing the design method described in reference [16] with an approximate method [8] for different value of γ and M_E.

Figs 6a, 6b, 6c, and 6d represent the contours of the plug nozzles generated by the design method described in reference [16] for different M_E design Mach and different heat capacity ratio γ.

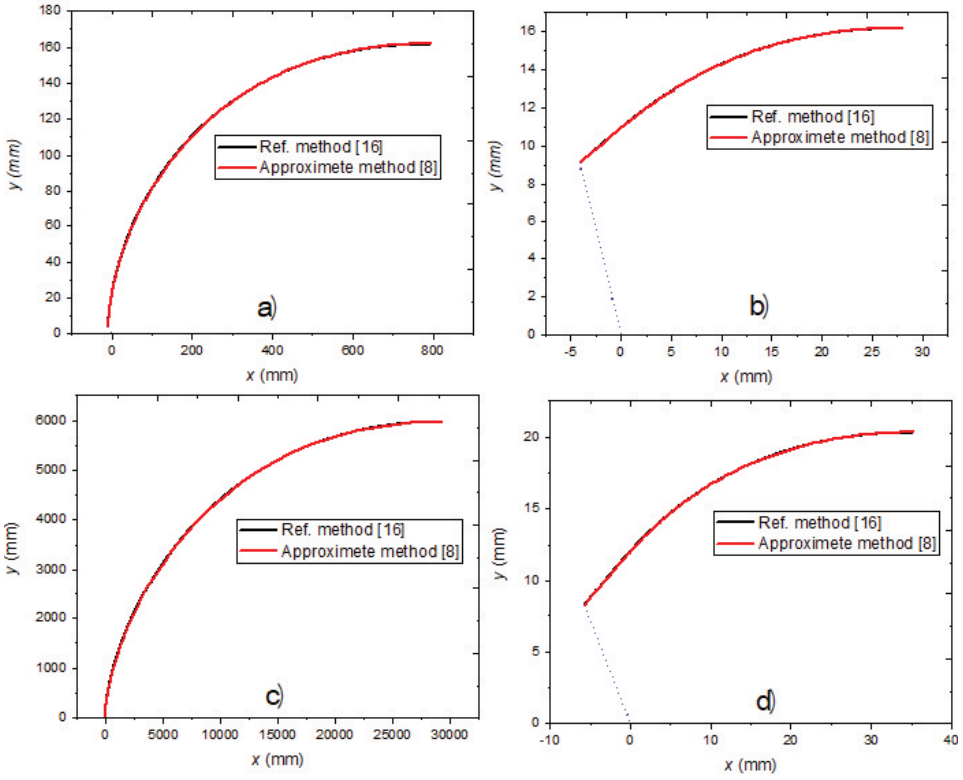

Fig. 6a The contour of the nozzle for M_E = 5.0 and γ = 1.5 b) The contour of the nozzle for M_E = 2.0 and γ = 1.5 c) The contour of the nozzle for M_E = 5.0 and γ = 1.1, d) The contour of the nozzle for M_E = 2.0 and γ = 1.1

A very good agreement is observed on the contours except for the last part of the contour, where there is a difference between the profiles. Fig. 7 and the following table show this difference.

Tab. 4 represents a comparison of the *y*-coordinates for each of the references [16] and [8] for the last part of the contour. This comparison was quite satisfactory since the results of both methods are very similar and the margin of error does not exceed 0.07 %.

Tab. 4 A comparison of the y-coordinates for each of the references [16] *and* [8]

x [mm]	y [mm] for reference [8]	y [mm] for reference [16]	Error [%]
20.7900	15.9272	15.9172	0.06296
21.1803	15.9559	15.9457	0.06370
21.5750	15.9831	15.9728	0.06439
21.9740	16.0087	15.9983	0.06507
22.3775	16.0329	16.0223	0.06562
22.7853	16.0554	16.0448	0.06612
23.1977	16.0763	16.0656	0.06667
23.6146	16.0956	16.0848	0.06716
24.0360	16.1132	16.1023	0.06760
24.4621	16.1291	16.1182	0.06808
24.8929	16.1433	16.1322	0.06848
25.3284	16.1557	16.1446	0.06888
25.7687	16.1663	16.1551	0.06924
26.2138	16.175	16.1638	0.06955
26.6637	16.1819	16.1706	0.06977
27.1186	16.1868	16.1755	0.06983
27.5785	16.1898	16.1785	0.06978
28.0434	16.1908	16.1796	0.06945

4.3 Validations with Experimental Results

For the experimental comparison, we used the results of the future European space transport investigation program (FESTIP) [26].

We used two configurations:

- a nozzle with design Mach number $M_E = 4.23$ and with a truncation of 40 % of its ideal length,
- a nozzle with design Mach number $M_E = 4.23$ and with a truncation of 20 % of its ideal length.

The analysis of flow for the Plug nozzle was done using ANSYS Fluent. The k-w SST model was used as the turbulence model. The baseline solver was selected as a double-precision density-based coupled solver with Implicit Time Integration. Least-square cell-based gradient is used for spatial discretization in which the solution was assumed to vary linearly was used and a second-order upwind scheme was used for interpolating the values of pressure, momentum, turbulent kinetic energy, specific dissipation rate,

and energy. The computational analysis was conducted under steady conditions. The initialization for steady-state problem was done using full multigrid (FMG) initialization to get the initial solution, and the inlet boundary was provided to give the reference value. Sutherland equation is used for calculating the viscosity of air.

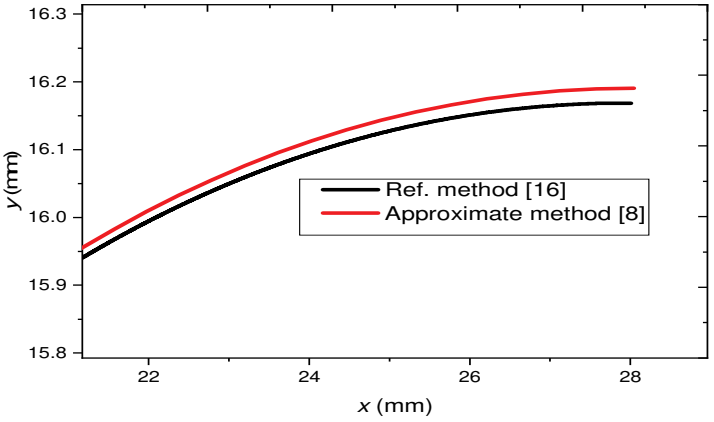

Fig. 7 Last part of contours for $M_E = 2.0$ *and* $\gamma = 1.5$

In Figs 8-13 the contours of the Mach number are presented for various P_R for a 20 % annular plug length.

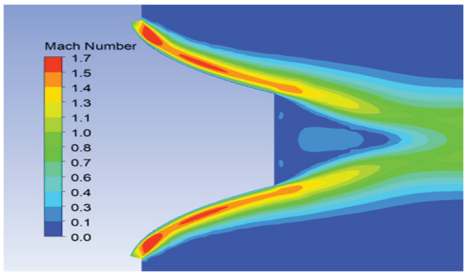

Fig. 8 Mach contours for 20 % *length at* $P_R = 12.3$

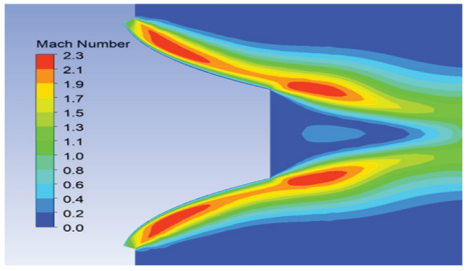

Fig. 9 Mach contours for 20 % *length at* $P_R = 12.3$

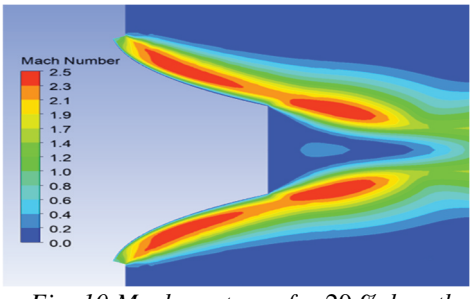

Fig. 10 Mach contours for 20 % *length at* $P_R = 16.4$

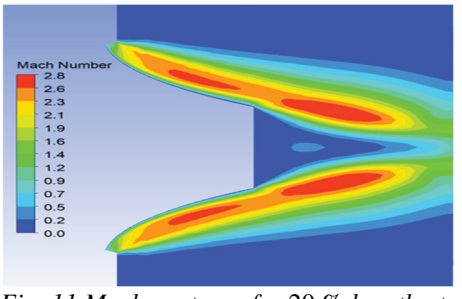

Fig. 11 Mach contours for 20 % *length at* $P_R = 22.3$

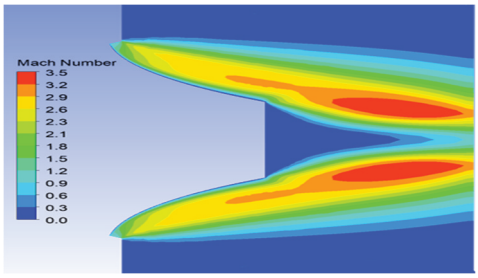

Fig. 12 Mach contours for 20 *% length at* P_R = 33.5

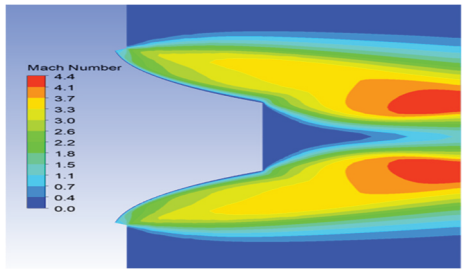

Fig. 13 Mach contours for 20 *% length at* P_R = 56.7

In Figs 14 and 15, the pressure ratio distributions on the plug surface from simulation and experiments are compared for both configurations, with l_{max} representing the Ideal Plug Length.

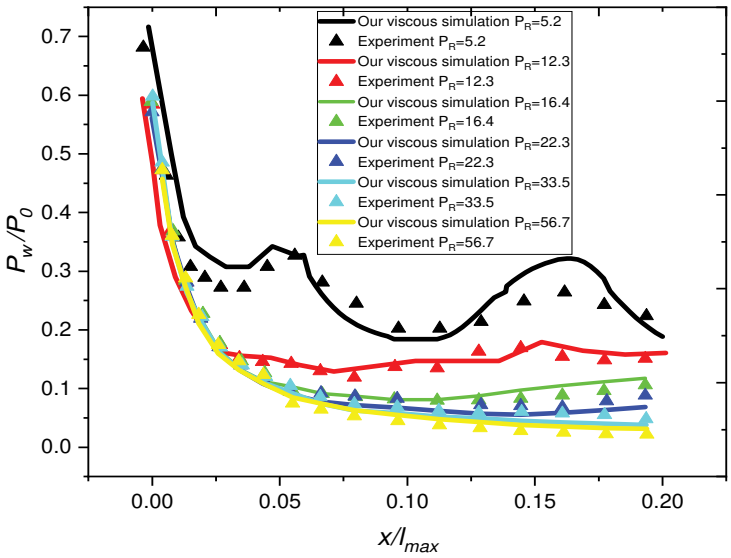

Fig. 14 Wall pressure distribution of 20 *% plug length model for different pressure ratios* P_R

Very similar results were found for the different P_R in both configurations, the error in all cases does not exceed 2.7 %. This difference may be justified by the difference between the approaches used. This proves the ability of CFD to accurately predict the flows in these types of nozzles. For a P_R closer to the design condition, the pressure decreases along the plug as shown in Figs 13 and 14, while for a P_R further from design conditions, a corrugated pressure distribution is observed due to the wave reflections. Note that for any value of P_R, the flow remains attached to the surface of the plug. This leads to improved performance in plug nozzles, which is not the case in the conventional nozzle (there is a separation of the flow on the wall).

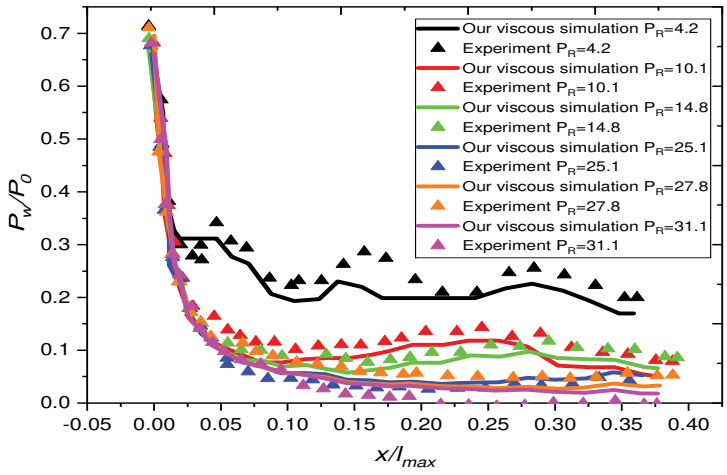

Fig. 15 Wall pressure distribution of 40 % *plug length model for different pressure ratios* P_R

5 Conclusion

The plug nozzle is an improved rocket nozzle which includes a centerbody or plug around which the working fluid flows. The main characteristics of this nozzle are its interaction with the external environment, which avoids the phenomenon of separation of flows that affects a nozzle with a conventional contour. These advantages derive from the generation of a gas expansion at the nozzle lip and its influence on the behavior of the pressure along the wall.

The present study is the first one devoted to the design of a profile of a plug nozzle using the method defined in reference [16]. The parameters of the flow (pressure and number of Mach) will then be evaluated and discussed for different Mach design and specific heat ratio γ. The validation of our results was done by comparing them with those obtained by the approximate method used in the reference [8]. This comparison was quite satisfactory since the results of both methods are very similar and the margin of error does not exceed 0.07 %.

Then a CFD study was conducted on this nozzle in both non-viscous and viscous cases using an appropriate turbulence (k-ω_sst) model and mesh. The results obtained were compared with those obtained by the numerical method but also with those of the experimental available in reference [26] for different truncation (20 % and 40 %) and different operating mode. A concordance of the results obtained was noted, the error in all cases did not exceed 2.7 %. This difference may be justified by the difference between the approaches used. This also confirms and demonstrates the ability of CFD (Simulation) solvers to accurately predict flows in this type of nozzles.

As far as prospective research is concerned, our study can be enriched by the addition of fluid injections in different position (throat, base of the nozzle) to see improved performance in different operating mode.

References

[1] HAGEMANN, G., H. IMMICH, T.V. NGUYEN and G.E. DUMNOV. Advanced Rocket Nozzles. *Journal of Propulsion and Power*, 1998, **14**(5) pp. 620-634. ISSN 0748-4658.

[2] TOMITA, T., N. KUMADA and A. OGAWARA. A Conceptual System Design Study for a Linear Aerospike Engine Applied to a Future SSTO Vehicle. In: *46th AIAA/ASME/SAE/ASEE Joint Propulsion Conference & Exhibit*. Nashville: 2010, pp. 5485-5492. DOI 10.2514/6.2010-7060.

[3] NASUTI, F. and M. ONOFRI. Methodology to Solve Flowfields of Plug Nozzles for Future Launchers. *Journal of Propulsion and Power*, 1998, **14**(3), pp. 318-326. ISSN 0748-4658.

[4] ARNOLD, G.A. *Jet-propulsion Nozzle for use at Supersonic Jet Velocities* [online]. Washington, 1954 [viewed 2021-01-12]. Available from: https://patentimages.storage.googleapis.com/de/46/26/8ff00295efc3bf/US2683962.pdf

[5] KRASE, W.H. *Performance Analysis of Plug Nozzles for Turbojet and Rocket Exhausts*. New York: American Society of Mechanical Engineers, 1959.

[6] HERMAN, K. and F.M. CRIMP Jr. Performance of Plug-type Rocket Exhaust Nozzles. *ARS Journal*, 1961, **31**(1), pp. 18-23. DOI 10.2514/8.5373.

[7] RAO, G.V.R. Spike Nozzle Contour for Optimum Thrust. *Planetary and Space Science*, 1961, **4**, pp. 92-101. DOI 10.1016/0032-0633(61)90125-8.

[8] ANGELINO, G. Approximate Method for Plug Nozzle Design. *AIAA Journal*, 1964, **2**(10), pp. 1834-1835. DOI 10.2514/3.2682.

[9] BALASAYGUN, E. *Experimental Analysis of Plug Nozzles* [online]. Arizona: The University of Arizona, 1964 [viewed 2021-01-09]. Available from: https://repository.arizona.edu/handle/10150/347480

[10] JOHNSON, G.R., H.D. THOMPSON and J.D. HOFFMAN. Design of Maximum thrust Plug Nozzles with Variable Inlet Geometry. *Computers & Fluids*, 1974, **2**(2), pp. 173-190. DOI 10.1016/0045-7930(74)90012-7.

[11] ROMMEL, T., G. HAGEMANN, C.-A. SCHLEY, G. KRULLE and D. MANSKI. Plug Nozzle Flowfield Analysis. *Journal of Propulsion and Power*, 1997, **13**(5), pp. 629-634. DOI 10.2514/2.5227.

[12] RUF, J. and P. McCONAUGHEY. A Numerical Analysis of a Three Dimensional Aerospike. In: *33rd Joint Propulsion Conference and Exhibit*. Huntsville: University of Alabama, 1997. DOI 10.2514/6.1997-3217.

[13] HAGEMANN, G., H. IMMICH and M. TERHARDT. Flow Phenomena in Advanced Rocket Nozzles - the Plug Nozzle. In: *34th AIAA/ASME/SAE/ASEE Joint Propulsion Conference and Exhibit*. Cleveland, 1998. DOI 10.2514/6.1998-3522.

[14] ITO, T., K. FUJII and A.K. HAYASHI. Computations of Axisymmetric Plug-Nozzle Flowfields: Flow Structures and Thrust Performance. *Journal of Propulsion and Power*, 2002, **18**(2), pp. 254-260. DOI 10.2514/2.5964.

[15] BESNARD, E., H. HU CHEN, T. MUELLER and J. GARVEY. Design, Manufacturing and Test of a Plug Nozzle Rocket Engine. In: *38th AIAA/ASME/SAE/ASEE Joint Propulsion Conference & Exhibit*. Indianapolis, 2002. DOI 10.2514/6.2002-4038.

[16] ZEBBICHE, T. Supersonic Plug Nozzle Design. In: *41st AIAA/ASME/SAE/ASEE Joint Propulsion Conference & Exhibit*. Tucson, 2005. DOI 10.2514/6.2005-4490.

[17] SHAHROKHI, A. and S. NOORI. Survey of the Central Plug Shape of the Aerospike Nozzle [online]. In: *17th Australasian Fluid Mechanics Conference.* Auckland, 2010 [viewed 2021-02-02]. Available from: https://vcscm.org.au/intranet/proceedings/17afmc_proceedings/PDF/300_Paper.pdf

[18] KARTHIKEYAN, N., A. KUMAR, S.B. VERMA and L. VENKATAKRISHNAN. Effect of Spike Truncation on the Acoustic Behavior of Annular Aerospike Nozzles. *AIAA Journal*, 2013, **51**(9), pp. 2168-2182. DOI 10.2514/1.J052139.

[19] CHUTKEY, K., B. VASUDEVAN, and N. BALAKRISHNAN. Analysis of Annular Plug Nozzle Flowfield. *Journal of Spacecraft and Rockets*, 2014, **51**(2), pp. 478-490. DOI 10.2514/1.A32617.

[20] SHANMUGANATHAN, V.K, N. GAYATHRI, S. KABILAN and K. UMANATH. Comparative Study on Performance of Linear and Annular Aero-Spike Nozzles. *Australian Journal of Basic and Applied Sciences*, 2015, **9**(11), pp. 883-892. ISSN:1991-8178.

[21] KUMAR, K.N., M. GOPALSAMY, D. ANTONY, R. KRISHNARAJ and B.V.V CHAPARALA. Design and Optimization of Aerospike Nozzle Using CFD. *IOP Conference Series: Materials Science and Engineering*, 2017, **247**, 012008. DOI 10.1088/1757-899X/247/1/012008.

[22] NAIR, P.P., A. SURYAN and H.D. KIM. Computational Study on Flow Through Truncated Conical Plug Nozzle with Base Bleed. *Propulsion and Power Research*, 2019, **8**(2), pp. 108-120. DOI 10.1016/j.jppr.2019.02.001.

[23] FERLAUTO, M., A. FERRERO and R. MARSILIO. Fluidic Thrust Vectoring for Annular Aerospike Nozzle. In: *AIAA Propulsion and Energy 2020 Forum*. Seatle: American Institute of Aeronautics and Astronautics, 2020. DOI 10.2514/6.2020-3777.

[24] ALSHIYA, K.S.A., M. SANTHOSH, V.K. SANTHOSH and S.S. GOPAL. Experimental Analysis of Jet Flow in an Aerospike Nozzle. *Materials Today: Proceedings*, 2021, **46**(9), pp. 3444-3450. DOI 10.1016/j.matpr.2020.11.783.

[25] KBAB, H., M. SELLAM, T. HAMITOUCHE, S. BERGHEUL and L. LAGAB. Design and Performance Evaluation of a Dual Bell Nozzle. *Acta Astronautica*, 2017, **130,** pp. 52-59. DOI 10.1016/j.actaastro.2016.10.015.

[26] IMMICH, H. and M. CAPORICCI. Status of the FESTIP Rocket Propulsion Technology Programme. In: *33rd Joint Propulsion Conference and Exhibit*. Seattle: American Institute of Aeronautics and Astronautics, 1997. DOI 10.2514/6.1997-3311.